Neutron star properties and the symmetry energy

Rafael Cavagnoli,[1,2] Debora P. Menezes,[1] and Constança Providência[2]
[1]*Departamento de Física - CFM - Universidade Federal de Santa Catarina, Florianópolis-SC-CP. 476-CEP 88.040-900 - Brazil*
[2]*Centro de Física Computacional, Department of Physics, University of Coimbra, P 3004-516 Coimbra, Portugal*
(Received 8 August 2011; published 27 December 2011)

The effect of the symmetry energy on the properties of compact stars is discussed. It is shown that, for stars with masses above $1M_\odot$, the radius of the star varies linearly with the symmetry energy slope L. We also analyze the dependence of the hyperon content and onset density of the direct Urca process on the symmetry energy and meson coupling parametrization.

DOI: 10.1103/PhysRevC.84.065810 PACS number(s): 21.65.−f, 25.75.Nq, 05.70.Fh, 12.38.Mh

I. INTRODUCTION

Constraining the high-density equation of state (EOS) of neutron-rich matter is essential to understand the physics of compact stars [1].

There have been recent attempts to set constraints on the high-density EOS using observational data obtained from compact stars [2,3], or microscopic calculations [4]. In particular, in Ref. [3] an empirical dense equation of state obtained from a heterogeneous set of six neutron stars with well-determined distances was proposed.

Phenomenological nuclear models are generally fit to the ground-state properties of nuclei and, frequently, also to the collective response of these systems [5–7], or nuclear matter saturation properties [8]. However, these constraints generally only determine quite uniquely the EOS close to saturation density and for an isospin asymmetry smaller than 0.2 [9,10]. Extrapolation to high densities and/or high isospin asymmetries is kept unconstrained and different models predict quite different neutron star properties.

In Ref. [11] it was proposed that the parametrization of the nuclear EOS could also be constrained by the collective response of nuclei to the isoscalar monopole giant resonance (ISGMR) and the isovector dipole giant resonance (IVGDR). The author of [11] has proposed that the ISGMR and IVGDR of ^{208}Pb were sensitive both to the incompressibility K and the symmetry energy $\epsilon_{\rm sym}$, due to its isospin asymmetry. Therefore, the ISMGR data from a nucleus with a well-developed breathing mode but a small neutron-proton asymmetry such as ^{90}Zr should be used to fix the incompressibility at saturation instead of a nucleus with a nonnegligible isospin asymmetry like ^{208}Pb. Once the incompressibility at saturation is fixed, the IVGDR ^{208}Pb may be used to constrain the symmetry energy.

This information together with the ground-state properties of nuclei has been used to define the Florida State University (FSU) parametrization proposed in Ref. [6]. However, since the high-density EOS is not constrained, FSU presents an EOS that is too soft at high densities and does not predict a star with a mass larger than $1.72M_\odot$, which is $0.25M_\odot$ below the mass $1.97 \pm 0.04\ M_\odot$ of the recent mass measurement of the binary millisecond pulsar PSR J16142230 [12]. In order to overcome this drawback, the parametrization [7] was built in a way close to FSU but including an extra constraint: the EOS is compatible with the empirical equation of state determined in Ref. [3]. As a result the new parametrization predicts stars with larger masses and smaller radii [7].

In the present work we want to understand how sensitive is the mass or radius curve of a family of stars to the symmetry energy and its slope at saturation. We study not only maximum-mass configurations but also stars with a mass in the range $1.0M_\odot < M < 1.4M_\odot$. These stars have a central density that goes from 1.5 ρ_0 to 2–3 ρ_0, and therefore we will be testing the equation of state at suprasaturation densities.

At high density the formation of hyperons is energetically favorable and therefore we also study the effect of the symmetry energy on the appearance of these exotic degrees of freedom [8,13]. We consider two different hyperon-meson parametrizations: a first one proposed in Ref. [8] and a second one that takes into account the different binding energies of the hyperons [14,15].

In Sec. II we present the formalism used in the present work, in Sec. III the results are presented and discussed, and in the last section conclusions are drawn.

II. THE FORMALISM

In the present section we present the hadronic equations of state (EOS) used in this work. We describe hadronic matter within the framework of the relativistic nonlinear Walecka model (NLWM) [16]. In this model the nucleons are coupled to neutral scalar σ, isoscalar-vector ω_μ, and isovector-vector $\vec{\rho}_\mu$ meson fields. We include a ρ-ω meson coupling term as in Refs. [6,7,17] in order to study the effect of the symmetry energy on the star properties while leaving the isoscalar channel fixed.

The Lagrangian density reads

$$\mathcal{L} = \sum_{j=1}^{8} \bar{\psi}_j \left[\gamma_\mu \left(i\partial^\mu - g_{\omega j}\omega^\mu - g_{\rho j}\vec{\tau}_j \cdot \vec{\rho}^{\,\mu}\right) - m_j^*\right]\psi_j + \sum_{l=1}^{2} \bar{\psi}_l (i\gamma_\mu \partial^\mu - M_l)\psi_l + \frac{1}{2}\partial_\mu\sigma\partial^\mu\sigma - \frac{1}{2}m_\sigma^2\sigma^2 - \frac{1}{3!}k\sigma^3 - \frac{1}{4!}\lambda\sigma^4 - \frac{1}{4}\Omega_{\mu\nu}\Omega^{\mu\nu} + \frac{1}{2}m_\omega^2\omega_\mu\omega^\mu$$

TABLE I. The σ and ω meson potentials for symmetric nuclear matter at saturation.

	NL3	GM1	GM3	NLρ	FSU	IU-FSU
V_σ (MeV)	377.15	281.34	206.28	234.68	358.94	359.15
V_ω (MeV)	305.46	215.71	145.45	171.10	282.42	276.84

$$+\frac{1}{4!}\xi g_\omega^4(\omega_\mu\omega^\mu)^2-\frac{1}{4}\vec{R}_{\mu\nu}\cdot\vec{R}^{\mu\nu}+\frac{1}{2}m_\rho^2\vec{\rho}_\mu\cdot\vec{\rho}^\mu$$
$$+\Lambda_{\rm v}\left(g_\rho^2\vec{\rho}_\mu\cdot\vec{\rho}^\mu\right)\left(g_\omega^2\omega_\mu\omega^\mu\right), \quad (1)$$

where $m_j^* = m_j - g_{\sigma j}\sigma$ is the baryon effective mass, $\Omega_{\mu\nu} = \partial_\mu\omega_\nu - \partial_\nu\omega_\mu$, $\vec{R}_{\mu\nu} = \partial_\mu\vec{\rho}_\nu - \partial_\nu\vec{\rho}_\mu - g_\rho(\vec{\rho}_\mu\times\vec{\rho}_\nu)$, g_{ij} are the coupling constants of mesons $i=\sigma,\omega,\rho$ with baryon j, m_i is the mass of meson i, and l represents the leptons e^- and μ^-. The couplings k ($k = 2M_N g_\sigma^3 b$) and λ ($\lambda = 6g_\sigma^4 c$) are the weights of the nonlinear scalar terms and $\vec{\tau}$ is the isospin operator. The sum over j in Eq. (1) extends over the octet of lightest baryons $\{n, p, \Lambda, \Sigma^-, \Sigma^0, \Sigma^+, \Xi^-, \Xi^0\}$.

We consider two different sets of hyperon-meson couplings. For the coupling set A the ω and ρ meson-hyperon coupling constants are obtained using SU(6) symmetry:

$$\tfrac{1}{2}g_{\omega\Lambda} = \tfrac{1}{2}g_{\omega\Sigma} = g_{\omega\Xi} = \tfrac{1}{3}g_{\omega N}, \quad (2)$$
$$\tfrac{1}{2}g_{\rho\Sigma} = g_{\rho\Xi} = g_{\rho N}, \quad g_{\rho\Lambda} = 0, \quad (3)$$

where N means "nucleon" ($g_{iN}\equiv g_i$). The coupling constants $\{g_{\sigma j}\}_{j=\Lambda,\Sigma,\Xi}$ of the hyperons with the scalar meson σ are constrained by the hypernuclear potentials in nuclear matter to be consistent with hypernuclear data [14]. The hypernuclear potentials were constructed as

$$V_j = x_{\omega j}V_\omega - x_{\sigma j}V_\sigma, \quad (4)$$

where $x_{ij}\equiv g_{ij}/g_i$, $V_\omega\equiv g_\omega\omega_0$ and $V_\sigma\equiv g_\sigma\sigma_0$ are the nuclear potentials for symmetric nuclear matter at saturation with the parameters of Table I. Following Ref. [14], we use

$$V_\Lambda = -28\ \text{MeV}, \quad V_\Sigma = 30\ \text{MeV}, \quad V_\Xi = -18\ \text{MeV}. \quad (5)$$

All hyperon coupling ratios $\{g_{\sigma j}, g_{\omega j}, g_{\rho j}\}_{j=\Lambda,\Sigma,\Xi}$ are now known once the coupling constants $\{g_\sigma, g_\omega, g_\rho\}$ of the nucleon sector are given.

However, while the binding of the Λ to symmetric nuclear matter is well settled experimentally [18], the binding values of the Σ^- and Ξ^- have still a lot of uncertainties. Experiments involving kaons and pions [19] and related Distorted Wave Impulse Approximation (DWIA) analyses [20] suggest that the Σ nuclear potential is repulsive (see also [21] for a recent review). Experimental data for the isoscalar Σ potential seem to be compatible with $+30\pm20$ MeV [21]. There is not much experimental information on the interaction of Ξ with nuclear matter. Measurements from the production of Ξ in the ^{12}C$(K^-, K^+)^{12}_{\Xi}$Be are compatible with a shallow attractive potential $V_\Xi\sim-14$ MeV [22]. Taking for the Ξ a less attractive potential or for the Σ an even more repulsive potential would reduce the fraction of hyperons in stellar matter.

Therefore, in order to show how results are sensitive to the hyperon couplings we consider set B defined as proposed in Ref. [8] with $x_\sigma = 0.8$ and equal for all the hyperons. We obtain the fraction x_ω from Eq. (4) with $V_j = V_\Lambda = -28$ MeV, and take the same value for all the hyperons. For the hyperon-ρ-meson coupling we consider $x_\rho = x_\sigma$. This choice of coefficients has been shown to give high maximum-mass configurations [23] which could describe the millisecond pulsar J1614-2230 mass [12].

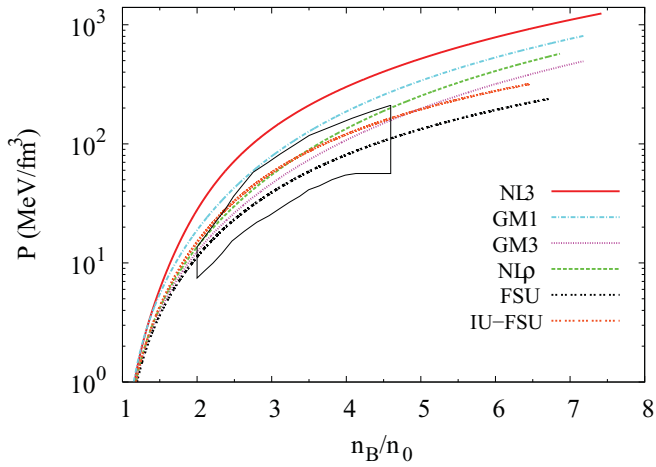

FIG. 1. (Color online) EOS for symmetric matter and different models: pressure as a function of the baryon number density. The enclosed area represents experimental data according to Danielewicz *et al.* [25].

In Table II we give the symmetric nuclear matter properties at saturation density as well as the parameters of the models used in the present work.

The equations of state (EOS) are the standard relativistic mean-field equations known in the literature. In case of Eq. (1), the EOS are the same as presented in Ref. [9] for the hadronic case. The baryon number density is

$$n_B = \sum_{j=1}^{8} n_j, \quad (6)$$

where n_j is the baryon number density of baryon j at zero temperature,

$$n_j = \frac{1}{3\pi^2}k_{Fj}^3, \quad (7)$$

and k_{Fj} is the Fermi momentum of baryon j. For the sake of comparisons with symmetric nuclear matter ($n_B = n_p + n_n$), the symmetry energy is defined as

$$\mathcal{E}_{\rm sym} = \frac{1}{2}\left[\frac{\partial^2(\mathcal{E}/n_B)}{\partial\alpha^2}\right]_{\alpha=0} = \frac{k_F^2}{6E_F} + \frac{g_\rho^2}{4m_\rho^{*2}}n_B, \quad (8)$$

where $\mathcal{E}$ is the energy density obtained from Eq. (1) for $j = 1, 2$ and with no leptons, α is the asymmetry parameter $\alpha = (N-Z)/A = (n_n - n_p)/n_B$, $E_F = (k_F^2 + m^{*2})^{1/2}$ with $k_F = (3\pi^2 n_B/2)^{1/3}$, $m_\rho^{*2} = m_\rho^2 + 2\Lambda_{\rm v}g_\omega^2 g_\rho^2\omega_0^2$, and the slope of the symmetry energy is

$$L = \left[3n_B\frac{\partial\mathcal{E}_{\rm sym}}{\partial n_B}\right]_{n_B=n_0}. \quad (9)$$

TABLE II. Parameter sets used in this work and corresponding saturation properties.

	FSU [6]	IU-FSU [7]	NLρ [24]	NL3 [5]	GM1 [8]	GM3 [8]
n_0 (fm^{-3})	0.148	0.155	0.160	0.148	0.153	0.153
K (MeV)	230	231.2	240	271.76	300	240
m^*/m	0.62	0.62	0.75	0.60	0.70	0.78
m (MeV)	939	939	939	939	938	938
$-B/A$ (MeV)	16.3	16.4	16.0	16.299	16.3	16.3
$\mathcal{E}_{\rm sym}$ (MeV)	32.6	31.3	30.5	37.4	32.5	32.5
L (MeV)	61	47.2	85	118	94	90
m_σ (MeV)	491.5	491.5	512	508.194	512	512
m_ω (MeV)	782.5	782.5	783	783	783	783
m_ρ (MeV)	763	763	763	763	770	770
g_σ	10.592	9.971	8.340	10.217	8.910	8.175
g_ω	14.302	13.032	9.238	12.868	10.610	8.712
g_ρ	11.767	13.590	7.538	8.948	8.196	8.259
b	0.000756	0.001800	0.006935	0.002052	0.002947	0.008659
c	0.003960	0.000049	−0.004800	−0.002651	−0.001070	−0.002421
ξ	0.06	0.03	0	0	0	0
$\Lambda_{\rm v}$	0.03	0.046	0	0	0	0

When the hyperons are present we define the strangeness fraction

$$f_s = \frac{1}{3}\frac{\sum_j |s_j| n_j}{n_B}, \tag{10}$$

where s_j is the strangeness of baryon j and n_B in this case is given by Eq. (6).

III. RESULTS

In Figs. 1 and 2(a), the pressure of symmetric nuclear matter and the symmetry energy, respectively, are plotted for a large range of densities. In Fig. 1 we also include the experimental constraints obtained from collective flow data in heavy-ion collisions [25]. We have considered a wide range of models frequently used to study stellar matter or finite nuclei with quite different behaviors at high densities. Even though some of the models do not satisfy the constraints determined in Ref. [25], as a whole this set of models allows us to understand the influence of a hard or soft equation of state (EOS) and a hard or soft symmetry energy on the star properties.

We have considered the following parametrizations: NL3 [5], with a quite large symmetry energy and incompressibility at saturation and which was fit in order to reproduce the ground state properties of both stable and unstable nuclei. FSU [6], which was accurately calibrated to simultaneously describe the GMR in ^{90}Zr and ^{208}Pb and the IVGDR in ^{208}Pb and still reproduce ground-state observables of stable and unstable nuclei. FSU is very soft at high densities, therefore the authors of [7] have proposed a parametrization with similar properties, which they call Indiana University-FSU (IU-FSU), having a harder behavior at high densities. GM1 and GM3 [8] are generally used to describe stellar matter, with a symmetry energy not so hard as the one of NL3, and NLρ [24], which has been used to discuss the hadron-matter–quark-matter transition

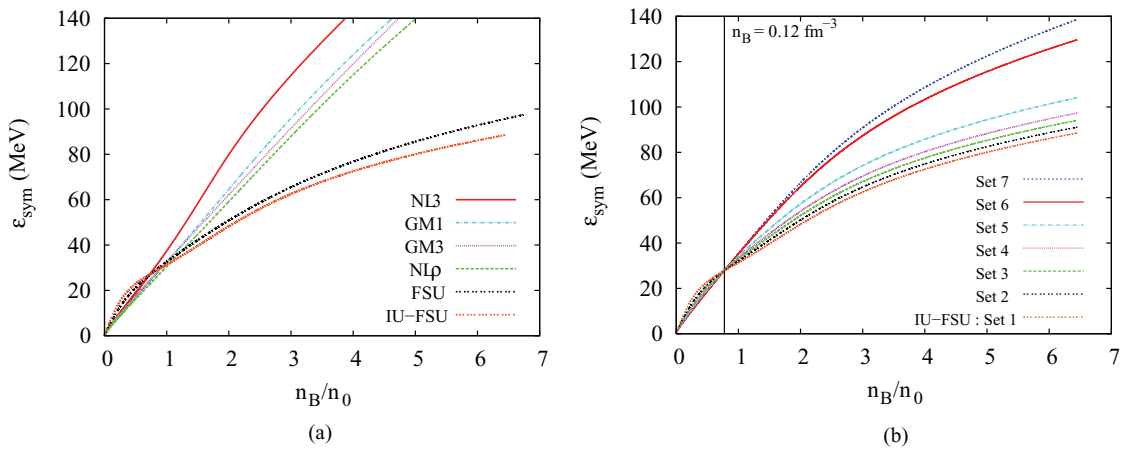

FIG. 2. (Color online) Symmetry energy as a function of the baryon number density (a) for different models and (b) for modified IU-FSU.

TABLE III. Parameter sets generated from the IU-FSU model (set 1) that differ in their value of the symmetry energy $\mathcal{E}_{\rm sym}$ and corresponding slope L at saturation but have the same isoscalar properties.

	Set 1	Set 2	Set 3	Set 4	Set 5	Set 6	Set 7
g_ρ	13.590	11.750	10.750	10.150	9.500	8.750	8.650
$\Lambda_{\rm v}$	0.0406	0.03643	0.02905	0.02354	0.01635	0.00598	0.00439
$\mathcal{E}_{\rm sym}$ (MeV)	31.34	32.09	32.74	33.26	34.00	35.21	35.41
L (MeV)	47.20	55.09	62.38	68.73	78.45	96.02	99.17

in Ref. [26], and that has, at high densities, a behavior between GM1 and GM3.

In order to study the effect of the isovector channel in the star properties we also consider a modified version of the IU-FSU parametrization: we keep the isoscalar channel and change g_ρ and $\Lambda_{\rm v}$ keeping the symmetry energy fixed at the density 0.12 fm^{-3}. It has been shown in Ref. [10] that phenomenological models fit to the properties of nuclei and nuclear matter have similar values of symmetry energy for this density. We generate a set of models that differ in their symmetry energy and corresponding slope at saturation, as indicated in Table III, but have the same isoscalar properties. In Fig. 2(b) we show the symmetry energy density dependence of this set of models. Set 1 is the parametrization IU-FSU. The other parametrizations have a larger symmetry energy and a larger slope L at saturation. The maximum value of L we considered is within the experimental values obtained from isospin diffusion in heavy-ion reactions [27]. The range of values considered for L span all the interval obtained for L from different analysis of experimental measurements [28] and a microscopic Brueckner Hartree-Fock calculation [29]. Smaller values of L would give unacceptable EOS because they would predict that neutron matter is bound.

The effect of the symmetry energy on the strangeness fraction is seen in Figs. 3 and 4. It is clear from these figures that the strangeness content is sensitive to the model and the meson-hyperon couplings. In general, the softer the EOS the larger the strangeness onset density and the smaller the strangeness content. From Fig. 4, we conclude that the smaller the symmetry energy the smaller the hyperon content. A large meson-hyperon vector coupling, as occurs in set B, hinders the formation of hyperons.

However, we should point out that, when comparing different models, we are comparing not only the effect of the density dependence of the symmetry energy but also the density dependence of the isoscalar channel (i.e., the incompressibility and effective mass). This explains why FSU, a softer EOS with a smaller incompressibility, has a smaller strangeness content than IU-FSU, a model with softer symmetry energy than FSU above the saturation density.

The EOS of the IU-FSU EOS becomes softer than GM3 (NLρ) for densities above $\sim 5n_0$ ($\sim 3.5n_0$); see Fig. 1. This explains why IU-FSU has a smaller hyperon content with respect to GM3 (set A) or GM3 and NLρ (set B) at high densities but not at intermediate densities. On the other hand, FSU is always softer than all the other EOSs and, for set B below $3n_0$ and $5n_0$, its strangeness fraction is larger than the corresponding fraction in the NLρ and GM3 models, respectively. This behavior is defined by the effective masses: NLρ and GM3 have larger effective masses (i.e., smaller g_s couplings) and, therefore, the chemical potential of the hyperons decreases slower with density and the onset occurs at larger densities. At large densities the sigma field saturates and the behavior of the system is defined by the vector meson.

We also comment on the behavior of NL3 with set B: NL3 is a model that breaks down at quite low densities when hyperons are included because the effective mass of the nucleons goes to zero ($n_B \sim 4n_0$); see Ref. [30]. This explains why the NL3 curve in Fig. 3(b) stops below $4n_0$.

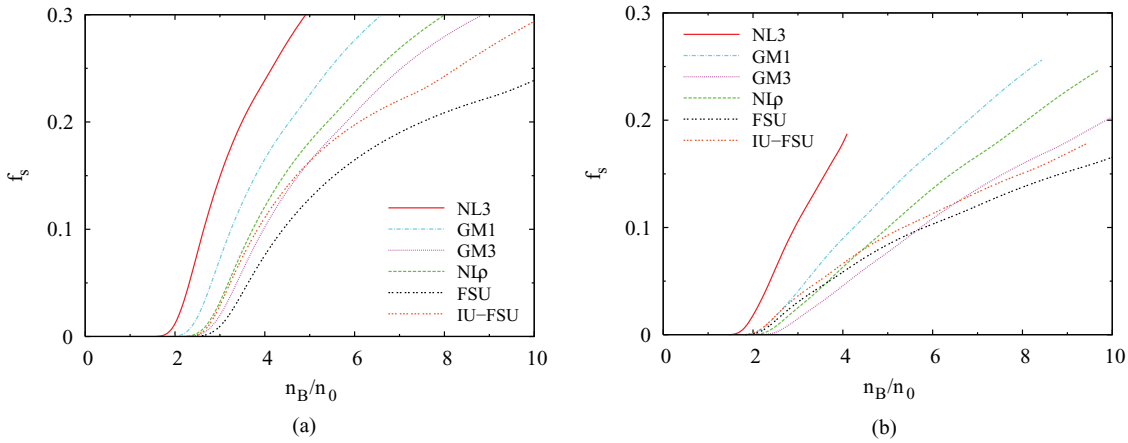

FIG. 3. (Color online) Strangeness fraction when hyperons are present for (a) set A and (b) set B.

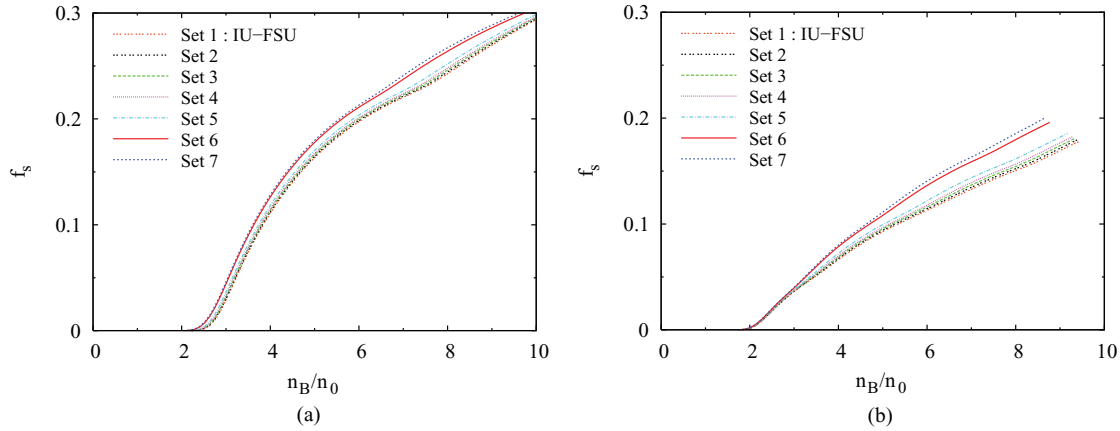

FIG. 4. (Color online) Strangeness fraction for IU-FSU and related parametrizations with (a) meson-hyperon coupling set A and (b) meson-hyperon coupling set B.

When comparing results with the modified versions of the IU-FSU model we are not changing the isoscalar channel. FSU has a softer EOS than IU-FSU (i.e., a smaller incompressibility at high densities). As a result, the formation of hyperons is hindered in FSU with respect to IU-FSU. The explanation is the difference on the isoscalar channel of these two models.

The symmetry energy is directly affecting the isovector chemical potential and, therefore, the chemical equilibrium. In Fig. 5, the chemical potential for neutral, positively charged, and negatively charged baryons in β equilibrium are represented. It is seen that the neutron chemical potential becomes slightly smaller for a softer symmetry energy, because the ρ-meson field is weaker. However, the density dependence of the symmetry energy has a stronger effect on the electron chemical potential: a smaller L corresponds to a smaller proton fraction and, therefore, electron fraction, so that the electron chemical potential decreases when L decreases. As a result, the sum $\mu_n + \mu_e$, which defines the chemical potential of single negatively charged baryons, feels a much stronger reduction than the neutron chemical potential, and the difference $\mu_n - \mu_e$, which defines the chemical potential of single positively charged baryons, increases above saturation density when L decreases.

As a consequence, a soft symmetry energy shifts the hyperon onset to larger densities, if Λ, a neutral hyperon with isospin zero, is the first hyperon to appear. This is the case of set A (see the left panel of Fig. 6). However, the onset of hyperons is not affected by L when a negatively charged hyperon such as Σ^- is the first hyperon to appear, such as, for instance, in set B (see the right panel of Fig. 6). Although the sum $\mu_n + \mu_e$ decreases, the same happens with the Σ^- chemical potential and the net result is that the onset of the hyperon Σ^- is almost independent of L. As soon as Λ appears, the different parametrizations of the modified IU-FSU start to differ.

In Tables IV–IX, we give the direct Urca onset density, mass and radius of maximum-mass stars, the radius of stars with $M = 1.0M_\odot$ and $1.4M_\odot$, the symmetry energy $\mathcal{E}_{\rm sym}$, and the symmetry energy slope L. Tables IV and V give this information for stars without hyperons. Tables VI and VIII give this information for stars with hyperons that couple to mesons through set A. Tables VII and IX give this information for stars with hyperons that couple to mesons through set B.

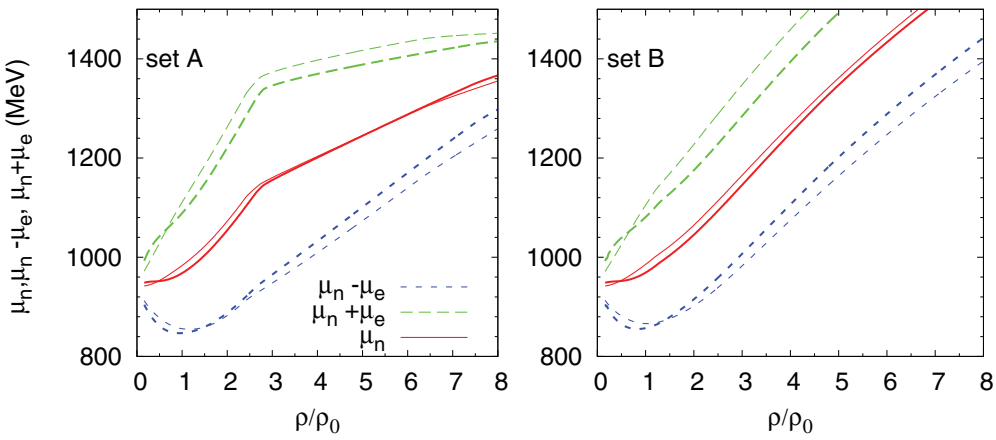

FIG. 5. (Color online) Chemical potential for neutral (full lines), positively charged (dotted lines), and negatively charged (dashed lines) baryons in β equilibrium: hyperon set A (left panel) and hyperon set B (right panel). The thick lines are for IU-FSU (set 1) and the thin lines are for set 7 of the modified IU-FSU.

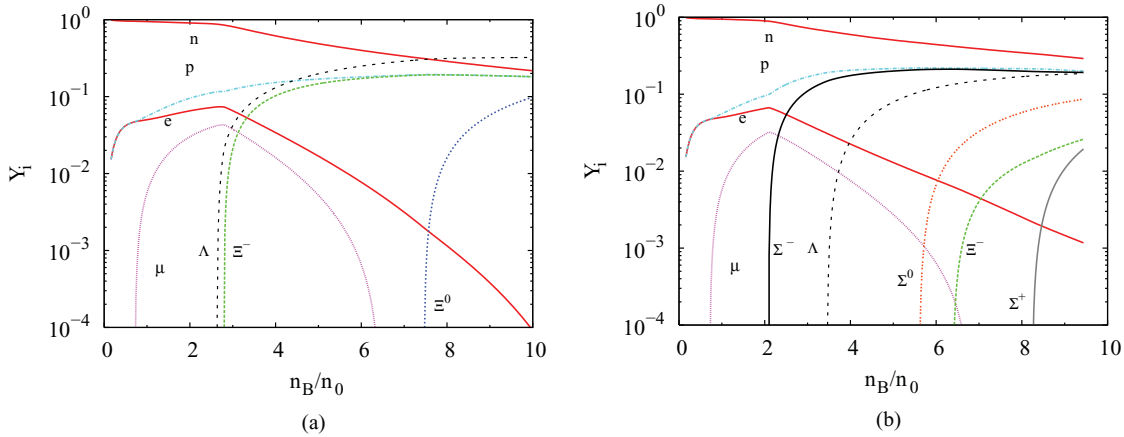

FIG. 6. (Color online) Particle fractions, IU-FSU for (a) set A and (b) set B.

The properties of stars obtained with models NL3, GM1, GM3, NLρ, FSU, and IU-FSU are given in Tables IV, VI, and VII, respectively, and the properties of stars from a set of EOS obtained from IU-FSU by changing the isovector channel are presented in Tables V, VIII, and IX.

Cooling of the star by neutrino emission can occur relatively fast if the direct Urca process, $n \to p + e^- + \bar{\nu}_e$, is allowed [31]. The direct Urca (DU) process takes place when the proton fraction exceeds a critical value $x_{\rm DU}$ [31], which can be evaluated in terms of the leptonic fraction as [32]

$$x_{\rm DU} = \frac{1}{1 + \left(1 + x_e^{1/3}\right)^3}. \tag{11}$$

where $x_e = n_e/(n_e + n_\mu)$ is the electron leptonic fraction, n_e is the number density of electrons, and n_μ is the number density of muons. Cooling rates of neutron stars seem to indicate that this fast cooling process does not occur and, therefore, a constraint is set imposing that the direct Urca process is only allowed in stars with a mass larger than $1.5M_\odot$, or a less restrictive limit, $1.35M_\odot$ [32]. Since the onset of the direct Urca process is closely related with the density dependence of the symmetry energy, this constraint gives information on the isovector channel of the EOS. In stellar matter with hyperons, the direct Urca process may also occur for the hyperons. As discussed in Ref. [33], although the neutrino luminosities in these processes are much less than the ones obtained in the nucleon direct Urca process, they will play an important role if they occur at densities below the nucleon direct Urca process. In particular, the process $\Lambda \to p + e + \bar{\nu}$ may occur at densities below the nucleon DU onset.

In Fig. 7 the proton fractions for β-equilibrium matter are plotted for NL3, GM1, GM3, FSU, and IU-FSU. The black region defines the proton fraction at the onset of the direct Urca process.

The effect of the symmetry energy and the hyperon content on the onset density of the nucleon direct Urca process is seen in Fig. 8 as function of the slope L for the IU-FSU and modified versions in the left panel and for the NL3, GM1, GM3, NLρ, FSU, and IU-FSU models in the right panel. We first analyze the effect of the symmetry energy slope on this quantity. We conclude that: (a) for matter without hyperons the larger the L the smaller the neutron-proton asymmetry above the saturation density and, therefore, the smaller the direct Urca onset density; (b) the larger the slope the smaller the onset density because a larger L corresponds to a harder symmetry energy and, therefore, larger fractions of protons are favored; (c) for a low value of L the presence of hyperons decreases the onset density. The effect of the inclusion of hyperons depends on the hyperon-meson coupling. With set A, Λ is the first

TABLE IV. Symmetry energy and no-hyperon star properties for NL3, GM1, GM3, FSU, and IU-FSU EOS. The onset density of the direct Urca process, symmetry energy slope and symmetry energy at saturation, mass and radius of the maximum-mass configuration, and radius of $1.4M_\odot$ and $1.M_\odot$ stars are given.

Set	$n_{\rm urca}/n_0$	L (MeV)	$\mathcal{E}_{\rm sym}$ (MeV)	$M_{\rm max}/M_\odot$	$R_{M_{\rm max}}$ (km)	$R_{1.4M_\odot}$ (km)	$R_{1.0M_\odot}$ (km)
NL3	1.38	118.0	37.4	2.81	13.38	14.71	14.65
GM1	1.81	94.0	32.5	2.39	11.99	13.81	13.76
GM3	2.04	90.0	32.5	2.04	10.94	13.12	13.38
NLρ	2.14	85.0	30.5	2.11	10.88	12.92	13.08
FSU	3.16	61.0	32.6	1.73	10.87	12.41	12.78
IU-FSU	3.95	47.2	31.3	1.95	11.23	12.55	12.51

TABLE V. Symmetry energy and no-hyperon star properties for IU-FSU modified EOS. The onset density of the direct Urca process, symmetry energy slope and symmetry energy at saturation, mass and radius of the maximum-mass configuration, and radius of $1.4M_\odot$ and $1.M_\odot$ stars are given.

Set	$n_{\rm urca}/n_0$	L (MeV)	$\mathcal{E}_{\rm sym}$ (MeV)	$M_{\rm max}/M_\odot$	$R_{M_{\rm max}}$ (km)	$R_{1.4M_\odot}$ (km)	$R_{1.0M_\odot}$ (km)
1	3.95	47.20	31.34	1.95	11.23	12.55	12.51
2	3.42	55.09	32.09	1.95	11.27	12.68	12.72
3	2.99	62.38	32.74	1.95	11.31	12.78	12.88
4	2.66	68.73	33.26	1.95	11.35	12.86	13.00
5	2.24	78.45	34.00	1.95	11.41	13.00	13.20
6	1.74	96.02	35.21	1.97	11.57	13.33	13.60
7	1.68	99.17	35.41	1.98	11.63	13.41	13.70

TABLE VI. Symmetry energy and star properties for NL3, GM1, GM3, FSU, and IU-FSU EOS and set *A* for the meson-hyperon couplings. The onset density of the direct Urca process, symmetry energy slope and symmetry energy at saturation, mass and radius of the maximum-mass configuration, and radius of $1.4M_\odot$ and $1.M_\odot$ stars are given.

Set	$n_{\rm urca}/n_0$	L (MeV)	$\mathcal{E}_{\rm sym}$ (MeV)	$M_{\rm max}/M_\odot$	$R_{M_{\rm max}}$ (km)	$R_{1.4M_\odot}$ (km)	$R_{1.0M_\odot}$ (km)
NL3	1.38	118.0	37.4	2.00	13.51	14.71	14.65
GM1	1.81	94.0	32.5	1.82	12.83	13.80	13.75
GM3	2.04	90.0	32.5	1.595	12.20	13.12	13.37
NLρ	2.14	85.0	30.5	1.594	11.94	12.91	13.08
FSU	3.51	61.0	32.6	1.375	11.95	–	12.79
IU-FSU	3.28	47.2	31.3	1.55	11.92	12.54	12.50

TABLE VIII. Symmetry energy and star properties for IU-FSU modified EOS and set *A* for the meson-hyperon couplings. The onset density of the direct Urca process, symmetry energy slope and symmetry energy at saturation, mass and radius of the maximum-mass configuration, and radius of $1.4M_\odot$ and $1.M_\odot$ stars are given.

Set	$n_{\rm urca}/n_0$	L (MeV)	$\mathcal{E}_{\rm sym}$ (MeV)	$M_{\rm max}/M_\odot$	$R_{M_{\rm max}}$ (km)	$R_{1.4M_\odot}$ (km)	$R_{1.0M_\odot}$ (km)
1	3.28	47.20	31.34	1.55	11.92	12.54	12.50
2	3.17	55.09	32.09	1.54	12.01	12.67	12.72
3	3.02	62.38	32.74	1.54	12.08	12.77	12.88
4	2.88	68.73	33.26	1.53	12.15	12.86	13.01
5	2.24	78.45	34.00	1.53	12.28	12.99	13.20
6	1.72	96.02	35.21	1.54	12.60	13.32	13.61
7	1.68	99.17	35.41	1.54	12.66	13.41	13.70

hyperon to appear, as can be seen in Fig. 6(a). With the onset of Λ, the neutron fraction decreases as well as the proton fraction. The behavior of the onset density for the DU depends on the balance between these two effects. In general the DU process is favored but, for a small range of L ($65 < L < 80$ MeV), the DU process may occur at densities larger than the values obtained for nucleonic matter. (d) The hyperon direct Urca may occur at densities below the onset of the nucleon direct Urca for set *A* if L is low enough ($L < 68$ MeV), as shown in the left panel of Fig. 8, where the green dots define the onset density of the process $\Lambda \to p + e + \bar{\nu}$.

For set *B*, Σ^- is the first hyperon to appear according to Fig. 6(b). With the onset of a negatively charged hyperon, Σ^- or Ξ^-, there is an increase of the proton fraction due to electrical neutrality as well as a decrease of the neutron fraction: both effects favor the DU onset.

In Figs. 9–11, the mass radius for the families of stars obtained, respectively, from the EOS without hyperons and from the EOS with the meson-hyperon sets *A* and *B* are shown. In the three figures, we show on the left panel the curves obtained with models NL3, GM1, GM3, NLρ, FSU, and IU-FSU, and in the right panel we show the curves for IU-FSU and the modified IU-FSU models. We also include the constrains obtained by [3] and the mass of the millisecond binary pulsar J1614-2230 [12]. For the crust of the star we have joined our EOS with the Negele and Vautherin EOS [34] for the inner crust and the Baym-Pethick-Sutherland (BPS) EOS [35] for the outer crust.

We discuss first the results without hyperons (Fig. 9). All the models except FSU are able to describe the pulsar J1614-2230. However, only IU-FSU and FSU satisfy the constrains on [3]. The set of relativistic mean-field (RMF) models chosen has quite different properties and is reflected in the differences between the models: the harder models like NL3 and GM1 predict larger masses and radii, the softer EOS, FSU, the smallest mass, the smaller the L the smaller the radius. This last property is clearly seen in the left panel of Fig. 12 were the radius of maximum-mass stars (squares), $1.4M_\odot$ stars (circles), and $1.0M_\odot$ stars (triangles) are plotted as a function of the symmetry energy slope for nucleonic stars. The full symbols are for the modified IU-FSU models and the empty symbols are for the NL3, GM1, GM3, NLρ, and FSU models. The modified IU-FSU models show that, if the isoscalar channel is left unchanged, the radius decreases if L decreases. This reduction is larger for $1.0M_\odot$ stars (more than 1 km for $45 < L < 100$ MeV) but even for the maximum-mass configurations there is still a 0.5 km difference. The set of RMF models chosen also show the same trend. However, since the isoscalar properties differ among the models, and they also affect the radius, the linear behavior is not present.

TABLE VII. Symmetry energy and star properties for NL3, GM1, GM3, FSU, and IU-FSU EOS and set *B* for the meson-hyperon couplings. The onset density of the direct Urca process, symmetry energy slope and symmetry energy at saturation, mass and radius of the maximum-mass configuration, and radius of $1.4M_\odot$ and $1.M_\odot$ stars are given.

Set	$n_{\rm urca}/n_0$	L (MeV)	$\mathcal{E}_{\rm sym}$ (MeV)	$M_{\rm max}/M_\odot$	$R_{M_{\rm max}}$ (km)	$R_{1.4M_\odot}$ (km)	$R_{1.0M_\odot}$ (km)
NL3	1.3827	118.0	37.4	2.43	13.51	14.71	14.65
GM1	1.8121	94.0	32.5	2.18	11.81	13.81	13.75
GM3	2.0370	90.0	32.5	1.88	11.05	13.12	13.38
NLρ	2.1389	85.0	30.5	1.91	10.92	12.89	13.09
FSU	2.4346	61.0	32.6	1.42	10.76	11.32	12.77
IU-FSU	2.4585	47.2	31.3	1.69	11.14	12.37	12.50

TABLE IX. Symmetry energy and star properties for IU-FSU modified EOS and set *B* for the meson-hyperon couplings. The onset density of the direct Urca process, symmetry energy slope and symmetry energy at saturation, mass and radius of the maximum-mass configuration, and radius of $1.4M_\odot$ and $1.M_\odot$ stars are given.

Set	$n_{\rm urca}/n_0$	L (MeV)	$\mathcal{E}_{\rm sym}$ (MeV)	$M_{\rm max}/M_\odot$	$R_{M_{\rm max}}$ (km)	$R_{1.4M_\odot}$ (km)	$R_{1.0M_\odot}$ (km)
1	2.4585	47.20	31.34	1.69	11.14	12.37	12.50
2	2.3916	55.09	32.09	1.69	11.20	12.46	12.71
3	2.3246	62.38	32.74	1.68	11.25	12.56	12.88
4	2.2577	68.73	33.26	1.68	11.29	12.64	13.01
5	2.1239	78.45	34.00	1.68	11.36	12.80	13.20
6	1.7225	96.02	35.21	1.69	11.57	13.18	13.63
7	1.6779	99.17	35.41	1.69	11.62	13.27	13.70

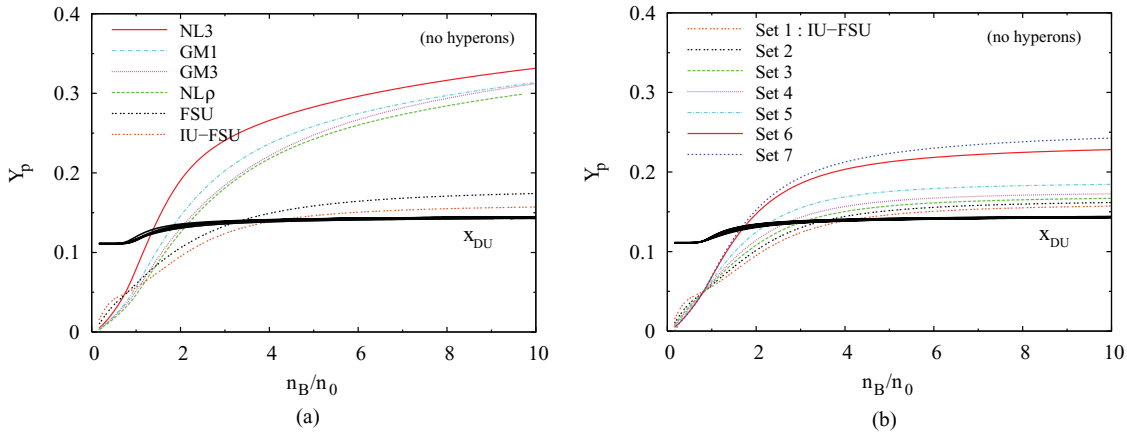

FIG. 7. (Color online) Onset of direct Urca process in stellar matter without hyperons: proton fraction for β-equilibrium matter and proton fraction at the onset of the direct Urca process (black region) (a) for NL3, GM1, GM3, NLρ, FSU, IU-F and (b) for modified IU-FSU.

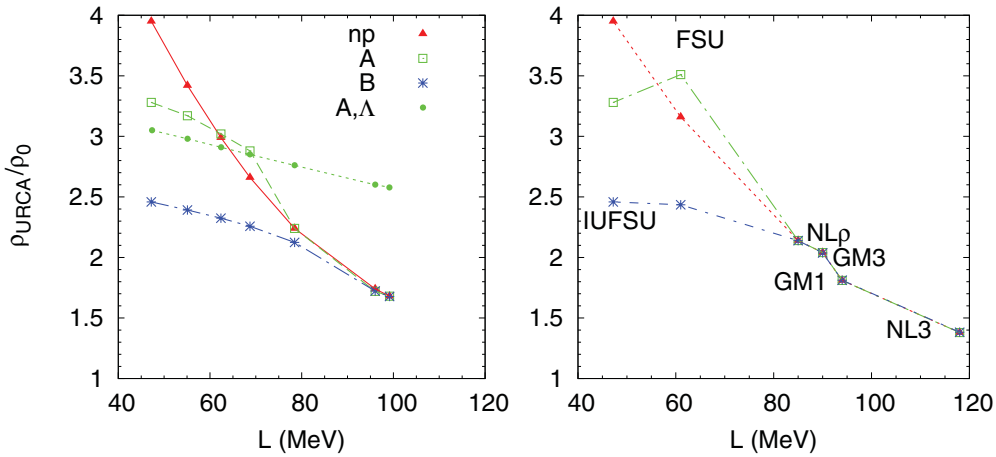

FIG. 8. (Color online) Onset of direct Urca process in stellar matter. Left panel corresponds to modified IU-FSU model and right panel corresponds to NL3, GM1, GM3, NLρ, FSU, and IU-FSU, for no-hyperon matter (red triangles), hyperon coupling set A (green squares) and hyperon coupling set B (blue stars). In the left panel the direct Urca process involving Λ is also shown (full dots). All the other data refer to the direct Urca process for protons and neutrons.

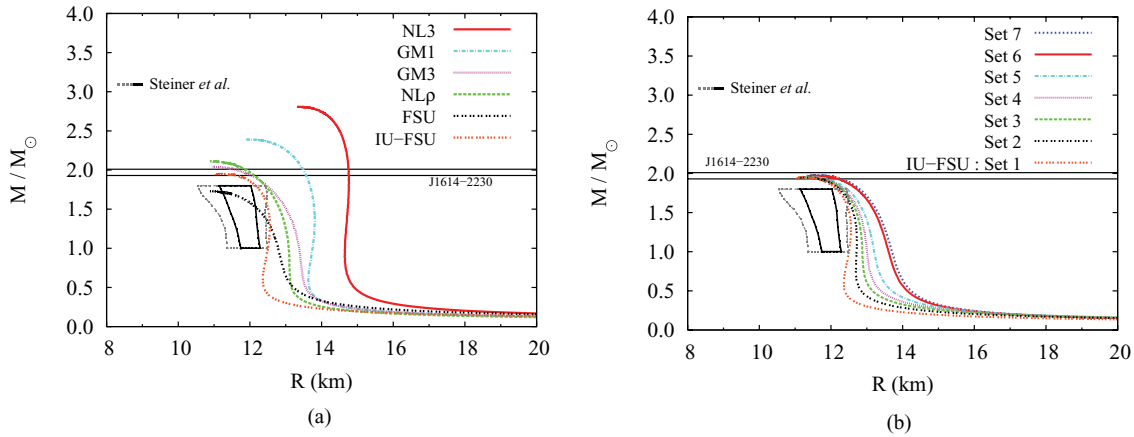

FIG. 9. (Color online) Mass-radius curves obtained for no-hyperon stellar matter EOS for (a) NL3, GM1, GM3, NLρ, FSU, and IU-FSU and for (b) IU-FSU and modified IU-FSU. The areas limited by the dotted gray and solid black curves are given by [3].

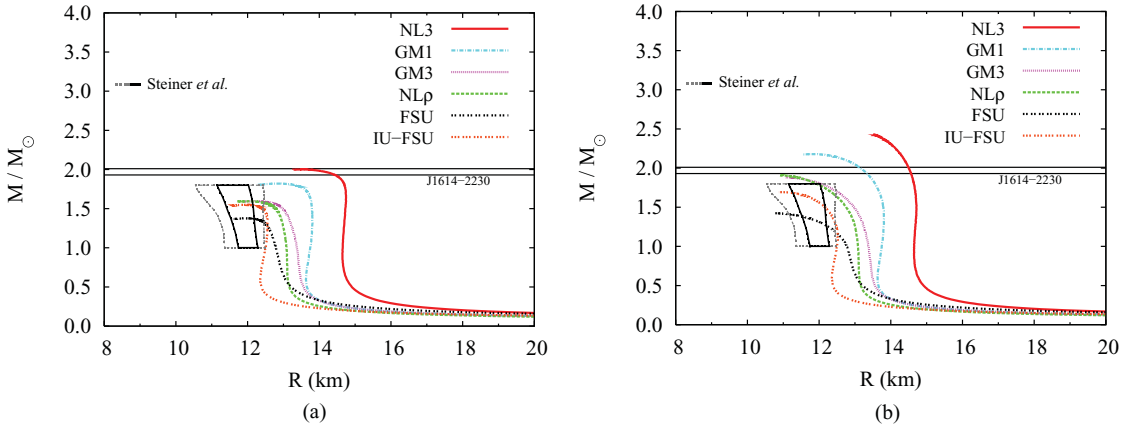

FIG. 10. (Color online) Mass-radius relations obtained for NL3, GM1, GM3, NLρ, FSU, and IU-FSU with the hyperon-meson coupling (a) set A and (b) set B.

Including hyperons in the EOS makes the EOS softer at large densities and the mass of the maximum-mass stars is smaller [36]. This is seen in Fig. 10 were the mass-radius curves obtained with hyperon-meson coupling sets A and B are plotted in the left and right panels, respectively. We conclude that it is important to have correct couplings since the star masses are sensitive to the hyperon couplings. For set A only the NL3 model is able to describe the PSR J1316-2230, while within set B NL3, GM1, GM3, and NLρ are able to describe a star with a mass $(1.97 \pm 0.4)M_\odot$. The trend discussed above between the star radius and L is still present in these stars; see the empty symbols in the middle and right panels of Fig. 12. This trend is confirmed by the modified IU-FSU models; see full symbols in the middle and right panels of Fig. 12. Stars with $1.0M_\odot$ and $1.4M_\odot$ contain no hyperons, or only a small fraction, and therefore their radii do not different from the results obtained for np matter. Maximum-mass stars, however, do have hyperons and their radii depend on the hyperon couplings chosen: for set A radius is larger and the maximum mass is smaller than the corresponding quantities predicted by set B. None of the models are able to describe PSR J1614-2230. We also conclude that the mass of the maximum-mass configuration is quite insensitive to the symmetry energy slope.

IV. CONCLUSIONS

In the present work we studied the effect of the density dependence of the symmetry energy on the star properties, namely, the hyperon content, DU, radius, and mass.

The study was performed within the RMF framework. We considered parametrizations which have been fit to the equilibrium properties of stable and unstable nuclei and/or dynamical response of nuclei, or to the saturation properties of symmetric nuclear matter. In order to test the density dependence of the symmetry energy we considered the IU-FSU parametrization. Keeping the isoscalar channel fixed, we changed the isovector channel in order to reproduce the values of the symmetry energy slope that were obtained from experimental measurements, $40 < L < 110$ MeV [27,28].

For the hadronic EOS, we considered two different parametrizations of the meson-hyperon couplings: in set A we considered the couplings that reproduce the binding energy of

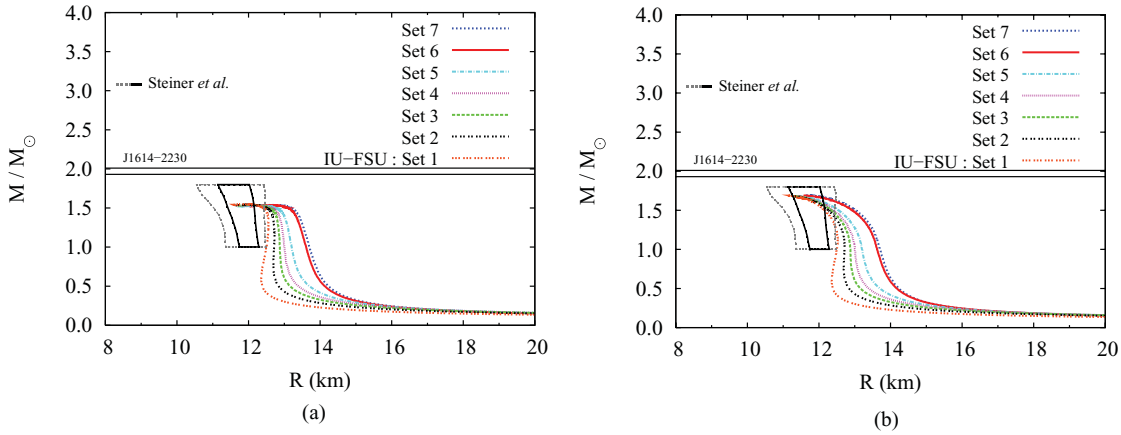

FIG. 11. (Color online) Mass-radius relations obtained with the modified IU-FSU and with the meson-hyperon coupling for (a) set A and for (b) set B.

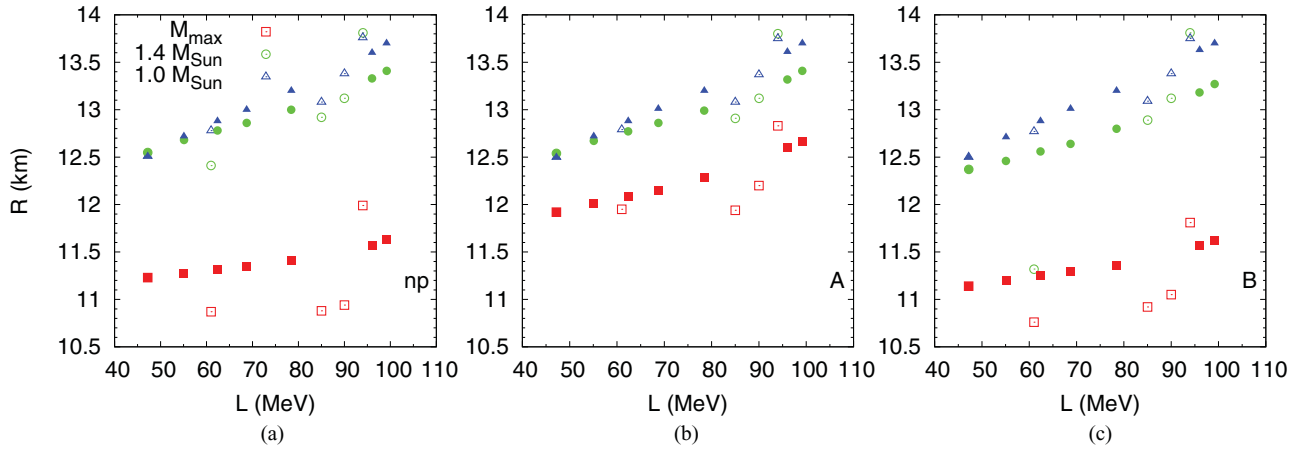

FIG. 12. (Color online) Star-radius dependence on the slope of the symmetry energy for stars with maximum mass (squares), $1.4M_\odot$ (circles), and $1M_\odot$ (triangles). The empty symbols are for the set of different models considered with hyperon coupling A. The full symbols are for the modified IU-FSU (a) with no hyperons, (b) with hyperons and for coupling A, and (c) with hyperons and for coupling B.

hyperons to symmetric nuclear matter; however, since only the binding energy of the Λ is well determined, we have also considered set B, which corresponds to the couplings proposed in Ref. [8] with $x_s = 0.8$. With set B and the GM1 parametrization of the RMF for the nuclear EOS, the authors of [23] could obtain a maximum-mass-star configuration of the order of the one recently measured by Demorest *et al.* [12].

We analyzed the effect of L on the radius of stars with $1M_\odot$, $1.4M_\odot$ and maximum-mass configurations. The first two cases correspond to stars that have a central baryonic density in the range $1.5\rho_0$ to $3\rho_0$ and therefore give information on the EOS just above the saturation densities. These densities will be probed at the GSI Facility for Antiproton and Ion Research (FAIR) [37].

We have concluded that the radius of the star is sensitive to the slope L, and, in particular, the smaller the value of the slope, the smaller the radius of the star. It was also shown that the density dependence of the symmetry energy affects the onset density of the direct Urca process: the smaller L, the larger the density. This can be understood because a smaller L at saturation corresponds to a softer symmetry energy at high densities, and, therefore, a smaller proton fraction. However, the DU onset also depends on the hyperon content and the hyperon-meson couplings. If Λ is the first hyperon to appear, the DU may be hindered or favored according to a balance between the neutron and proton reductions. However, if a negatively charged hyperon such as the Σ^- is the first hyperon to appear, there is a decrease of the neutron fraction and an increase of the proton fraction: both effects favor the DU onset.

It was also shown that the larger L, the larger the hyperon content because a larger L makes the EOS harder and, therefore, it is energetically favorable to have a larger hyperon fraction. However, this only occurs if the first hyperon to appear is the Λ. A delicate balance between the increase suffered by the chemical potential of the Σ^- and the neutron plus electron chemical potential may make the hyperon onset independent of L.

We also conclude that the total strangeness content is sensitive to the meson-hyperon couplings and stronger constraints on the determination of these constants are required. For larger hyperon-vector meson couplings we have obtained a smaller strangeness content.

According to recent estimates based on a microscopic non-relativistic approach, including hyperon degrees of freedom seems to make the EOS too soft even including three-body forces [38], so that at most star masses of $1.6M_\odot$ are attained, far from the very precise mass value recently measured [12]. More data on hypernuclei are required in order to clarify this point.

ACKNOWLEDGMENTS

This work was partially supported by CNPq (Brazil) and CAPES (Brazil)/FCT (Portugal) under project 232/09, by FCT (Portugal) under the Grants No. PTDC/FIS/113292/2009 and No. CERN/FP/109316/2009. R.C. is grateful for the warm hospitality at Centro de Física Computacional/FCTUC.

[1] James M. Lattimer and Madappa Prakash, Phys. Rep. **442**, 109 (2007).

[2] F. Özel, T. Güver, and D. Psaltis, Astrophys. J. **693**, 1775 (2009); F. Özel, G. Baym, and T. Guver, Phys. Rev. D **82**, 101301 (2010).

[3] A. W. Steiner, J. M. Lattimer, and E. F. Brown, Astrophys. J. **722**, 33 (2010).

[4] K. Hebeler, J. M. Lattimer, C. J. Pethick, and A. Schwenk, Phys. Rev. Lett. **105**, 161102 (2010).

[5] G. A. Lalazissis, J. König, and P. Ring, Phys. Rev. C **55**, 540 (1997).

[6] B. G. Todd-Rutel and J. Piekarewicz, Phys. Rev. Lett. **95**, 122501 (2005); F. J. Fattoyev and J. Piekarewicz, Phys. Rev. C **82**, 025805 (2010).

[7] F. J. Fattoyev, C. J. Horowitz, J. Piekarewicz, and G. Shen, Phys. Rev. C **82**, 055803 (2010).
[8] N. K. Glendenning and S. A. Moszkowski, Phys. Rev. Lett. **67**, 02414 (1991).
[9] Rafael Cavagnoli, Constança Providência, and Debora P. Menezes, Phys. Rev. C **83**, 045201 (2011).
[10] Camille Ducoin, Jérôme Margueron, Constança Providência, and Isaac Vidaña, Phys. Rev. C **83**, 045810 (2011).
[11] J. Piekarewicz, Phys. Rev. C **66**, 034305 (2002); **69**, 041301 (2004).
[12] Paul Demorest, Tim Pennucci, Scott Ransom, Mallory Roberts, and Jason Hessels, Nature (London) **467**, 1081 (2010).
[13] N. K. Glendenning, *Compact Stars* (Springer-Verlag, New York, 2000).
[14] J. Schaffner-Bielich and A. Gal, Phys. Rev. C **62**, 034311 (2000); J. Schaffner-Bielich, M. Hanauske, H. Stocker, and W. Greiner, Phys. Rev. Lett. **89**, 171101 (2002); E. Friedman and A. Gal, Phys. Rep. **452**, 89 (2007).
[15] M. Chiapparini, M. E. Bracco, A. Delfino, M. Malheiro, D. P. Menezes, and C. Providncia, Nucl. Phys. A **826**, 178 (2009).
[16] B. D. Serot and J. D. Walecka, Adv. Nucl. Phys. **16**, 1 (1986); J. Boguta and A. R. Bodmer, Nucl. Phys. A **292**, 413 (1977).
[17] C. J. Horowitz and J. Piekarewicz, Phys. Rev. Lett. **86**, 5647 (2001).
[18] D. J. Millerner, C. B. Dover, and A. Gal, Phys. Rev. C **64**, 044302 (2001); Y. Yamamoto, H. Bando, and J. Zofka, Prog. Theor. Phys. **80**, 757 (1998).
[19] S. Bart *et al.*, Phys. Rev. Lett. **83**, 5238 (1999); H. Noumi *et al.*, *ibid.* **89**, 072301 (2002); **90**, 024002 (2003); P. K. Saha *et al.*, Phys. Rev. C **70**, 044613 (2004).
[20] M. Kohno, Y. Fujiwara, Y. Watanabe, K. Ogata, and M. Kawai, Prog. Theor. Phys. **112**, 895 (2004); Phys. Rev. C **74**, 064613 (2006); T. Harada and Y. Hirabayashi, Nucl. Phys. A **759**, 143 (2005); **767**, 206 (2006).
[21] Avraham Gal, Prog. Theor. Phys. Suppl. **186**, 270 (2010).
[22] T. Fukuda *et al.*, Phys. Rev. C **58**, 1306 (1998); P. Khaustov *et al.*, *ibid.* **61**, 054603 (2000).
[23] I. Bombaci, P. K. Panda, C. Providência, and I. Vidana, Phys. Rev. D **77**, 083002 (2008).
[24] B. Liu, V. Greco, V. Baran, M. Colonna, and M. Di Toro, Phys. Rev. C **65**, 045201 (2002).
[25] P. Danielewicz, R. Lacey, and W. G. Lynch, Science **298**, 1592 (2002).
[26] M. Di Toro, B. Liu, V. Greco, V. Baran, M. Colonna, and S. Plumari, Phys. Rev. C **83**, 014911, (2011).
[27] L. W. Chen, C. M. Ko, and B. A. Li, Phys. Rev. Lett. **94**, 032701 (2005).
[28] A. Klimkiewicz *et al.*, Phys. Rev. C **76**, 051603 (2007); D. V. Shetty, S. J. Yennello, and G. A. Souliotis, *ibid.* **76**, 024606 (2007); M. B. Tsang, Y. Zhang, P. Danielewicz, M. Famiano, Z. Li, W. G. Lynch, and A. W. Steiner, Phys. Rev. Lett. **102**, 122701 (2009); M. Centelles, X. Roca-Maza, X. Viñas, and M. Warda, *ibid.* **102**, 122502 (2009); M. Warda, X. Viñas, X. Roca-Maza, and M. Centelles, Phys. Rev. C **80**, 024316 (2009); Andrea Carbone, Gianluca Colò, Angela Bracco, Li-Gang Cao, Pier Francesco Bortignon, Franco Camera, and Oliver Wieland, *ibid.* **81**, 041301(R) (2010).
[29] Isaac Vidaña, Constança Providência, Artur Polls, and Arnau Rios, Phys. Rev. C **80**, 045806 (2009).
[30] A. M. S. Santos and D. P. Menezes, Phys. Rev. C **69**, 045803 (2004).
[31] J. M. Lattimer, C. J. Pethick, M. Prakash, and P. Haensel, Phys. Rev. Lett. **66**, 2701 (1991).
[32] T. Klähn *et al.*, Phys. Rev. C **74**, 035802 (2006).
[33] M. Prakash, M. Prakash, J. M. Lattimer, and C. J. Pethick, Astrophys. J. **390**, L77 (1992).
[34] J. W. Negele and D. Vautherin, Nucl. Phys. A **207**, 298 (1973).
[35] G. Baym, C. Pethick, and D. Sutherland, Astrophys. J. **170**, 299 (1971).
[36] M. Prakash, I. Bombaci, M. Prakash, P. J. Ellis, J. M. Lattimer, and R. Knorren, Phys. Rep. **280**, 1 (1997).
[37] S. Chattopadhyay, J. Phys. G **35**, 104027 (2008); P. Senger *et al.*, *ibid.* **36**, 064037 (2009); CBM Collaboration, Johann M. Heuser, Nucl. Phys. A **830**, 563c (2009) [http://www.gsi.de/fair].
[38] I. Vidaña, D. Logoteta, C. Providência, A. Polls, and I. Bombaci, Europhys. Lett. **94**, 11002 (2011).